On-line System Identification of Power System Linear Models

J. A. Moreno-Corbea*, M.R.A. Paternina*, D. Rodales†, R. Reyes‡, F. Zelaya§, A. Zamora†, C. Toledo¶, C. Castrillón‖, and A. Sánchez**

*UNAM, Mexico City, †U. Michoacana, Morelia, Mexico,
‡U. Nuevo León, §UTK, Knoxville, TN, USA, ¶UIS, Bucaramanga, Colombia, ‖UNAL, Medellín, Colombia, **Cinvestav, Guadalajara, Mexico

***Abstract*—This paper deals with the provision of adequate testing simulation environments to facilitate the evaluation of new system identification techniques to enhance power system stability. It develops and implements a testing architecture for online system identification approaches, taking advantage of the use of two well-known computational programs (Matlab™ and DIgSILENT PowerFactory™). To ensure a reliable and optimal system identification, this platform exploits a mutually beneficial relationship among four well-established mathematical techniques (discrete Fourier transform, Teager-Kaiser energy operator, the fast Fourier transform, and eigensystem realization algorithm). Their symbioses can capture the synchrophasor information, detect the right disturbance instant, optimally extract the dominant frequency, and properly identify the Markov parameters that assemble the descriptor form of Multiple-Input and Multiple-Output (MIMO) linear systems for modeling modern power grids. Numerical results unveil the potential for recreating the real behavior of power systems; in particular, the proposed architecture can deal with any system identification technique to be tested.**

***Index Terms*—Online system identification, eigensystem realization algorithm, Teager-Kaiser energy operator, phasor estimation, disturbance detection instant, frequency computation.**

I. Introduction

Power system stability has always been one of the main concerns of researchers and engineers. This concern has increased due to the fast changes in the power grid, i.e. the increase of renewable energy penetration and electronically-interfaced resources, the reduction of the system inertia, the decommissioning of traditional synchronous generators, and the active demand participation [1], [2]. At the same time, new investigations are carried out to deal with these concerns; thus many research institutions and industries are working towards proposing new theories and solutions to enhance power system stability. However, one of the main challenges is the necessity for adequate testing tools or environments that allows testing/assessing these new solutions.

One of the most problematic issues on power system stability is the appearance of low-frequency electromechanical oscillations (LFEOs) in the transmission grid. Since LFEOs constrain the power transfer between transmission tie-lines and provoke cascading events that could lead to total or partial blackouts. Moreover, LFEOs have been exacerbated by the inertia reduction and the decommissioning of power plants with power system stabilizers (PSS) [2]. To counteract these issues, new control approaches have been proposed to enhance traditional damping controllers (DC) and provide wide-area damping controllers with adaptable structures and online implementations [3]. Most of them make use phasor measurement units (PMUs) which rely on accurate and efficient algorithms to estimate synchrophasors that can be used in control stages [4]; also, some of these approaches use system identification techniques, which allow capturing dominant modes and model plants for the controller's design [5], [6].

All the above concepts can be wrapped out in the online identification of power system linear models and their use for the controllers' design. Many works proposing novel architectures have been presented [3], [6]–[8]; however, there is still a big gap between theory and real implementations. As an intermediate stage, an alternative for researchers and engineers is the software-based solutions that provide the capabilities to emulate real systems to develop and test new algorithms and solutions for real power grids.

The novelty of this work lies in providing a framework for testing state-of-the-art algorithms involved in the power system identification process. Commonly, new algorithms are tested using synthetic data, and time-series data from simulations or the real world. However, they prevent interaction with other algorithms used in the system identification process. Aiming to add an extra layer of complexity and make this process more realistic, this framework also considers the synchrophasor estimation, disturbance detection, and the sizing of the analysis window. Due to this, two main contributions are provided: (*i*) The online identification of power system linear models' through an adaptable window of analysis; and (*ii*) A testing architecture for online system identification approaches by using Matlab™ and DIgSILENT PowerFactory™. The former is obtained using an adaptable analysis window, provided by the use of the Teager-Kaiser energy operator (TKEO) [9], [10]. This ensures the power system identification through an optimal window of analysis. Meanwhile, the latter is a simulation environment to test algorithms and their interaction, which considers phasor estimation, disturbance detection, ringdown analysis, and system identification. Moreover, this framework could also be used for the design of new wide-area damping controllers using online system identification approaches [11].

II. On-line system identification: Fundamentals

This section describes the mathematical aspects and algorithms used in the proposed structure. It is important to highlight that these algorithms could be changed to test new techniques or approaches regarding phasor measurement and system identification.

A. Synchrophasor estimation and frequency computation

A non-recursive discrete Fourier transform (DFT) is responsible to extract the synchrophasor information and frequency computation from the positive-sequence voltage signals [12]. The DFT uses the Fourier matrix $\mathbf{W}_N$ and its harmonic phase factors $\omega_N^h = e^{j2\pi/N}$ [13]. To process multiple channels, the multivariate analysis equation in (1) is used.

$$\begin{bmatrix}\hat{\xi}_1 & \hat{\xi}_2 & \cdots & \hat{\xi}_m\end{bmatrix} = \mathbf{W}_N^{\dagger}\begin{bmatrix}s_1 & s_2 & \cdots & s_m\end{bmatrix} \tag{1}$$

where $\tilde{\xi} = \begin{bmatrix}\hat{\xi}_1 & \hat{\xi}_2 & \cdots & \hat{\xi}_m\end{bmatrix}$ stands for the Fourier coefficients. Then, the synchrophasor information is determined by extracting the magnitude and phase of the coefficients associated with the fundamental frequency, as follows:

$$\hat{a} = \left|\tilde{\xi}\right|, \hat{\varphi} = \angle\tilde{\xi} \tag{2}$$

On the other hand, the frequency computation is implemented according to IEEE Std. C37.118.1, where it is conceived as the first derivative of the phase angle, as follows [14], [15]:

$$f(t) = f_0 + \Delta f(t), \tag{3}$$

where f_0 is the fundamental frequency and $\Delta f(t)$ is the deviation of frequency from nominal given by

$$\Delta f(t) = \frac{1}{2\pi}\left[\frac{\hat{\varphi}_{a1,k} - \hat{\varphi}_{a1,k-1}}{\Delta t}\right], \tag{4}$$

M.R.A. Paternina acknowledges financial support from the Project Support Program for Research and Technological Innovation of UNAM (DGAPA, PAPIIT-2021-2022/2023-2025) through the projects TA101421 and IT102723.

where $\hat{\varphi}$ is the positive-sequence phasor angle, k indicates the actual iteration processed in the simulation, and $\Delta(t)$ corresponds to the window time between each synchrophasor estimated.

B. Disturbance time detection

The detection instant is carried out through the l^{th}-order Teager-Kaiser energy operator (TKEO). The TKEO has proven its effectiveness in some applications including event detection in non-stationary signals as performed in [16], where an event is evaluated under damped and undamped signals, also signals with ambient noise and real signals. This nonlinear energy operator for continuous-time and discrete-time signals was developed by Teager [17] and later introduced by Kaiser [9].

Based on Newton's second law of motion, applied to a model of mass suspended by a spring of constant force, Teager in [9] obtains the solution of the energy calculation (Ψ) of the second-order model as the sum of the potential and kinetic energy as

$$\Psi_2 \propto A^2\omega^2 \tag{5}$$

where A is the amplitude of oscillation and ω stands for the frequency of the oscillation. $s_k(n)$ is an oscillating signal defined by

$$s_k(n) = A\cos(\Omega n+\phi) \tag{6}$$

where Ω corresponds to the digital frequency in radians/sample and is given by $\Omega = 2\pi f/f_s$, where f is the analog frequency, f_s denotes the sampled frequency, and ϕ stands for the arbitrary initial phase given in radians. Given three parameters (A, Ω and ϕ) in (6), these values are derived by solving the system and considering adjacent equally-spaced samples of $s_k(n)$ for each parameter. Thus, by substituting $s_k(n)$ in (5), the second-order operator is given by

$$\Psi_2 = s_k^2(n) - s_k(n-1)s_k(n+1) = A^2\sin^2(\Omega) \approx A^2\Omega^2 \tag{7}$$

Then, the l^{th}-order discrete energy operator can be defined by [18]

$$\Psi_l[s_k(n)] = s_k(n)s_k(n+l-2) - s_k(n-1)s_k(n+l-1) \tag{8}$$

The discrete-time energy operator for the second order is expressed by

$$\Psi_2[s_k(n)] = s_k^2(n) - s_k(n-1)s_k(n+1). \tag{9}$$

The online application of the second-order TKEO is implemented in **Algorithm 1** to detect the right disturbance instant t_{dist}.

C. Selection of the optimal window length and dominant frequency

To select the optimal analysis window, we implement a size-controlled strategy that seeks to determine the crossings by the steady-state. Thus, all changes around the steady-state are tracked until obtaining the number of crossings that define the optimal window length.

The strategy is implemented by employing the **Algorithm 2**, where the k-th package of a set of m signals is assembled into the buffer $ident_w(k)$ with the purpose of detecting each new crossing. Thus, when the processed signal changes its value between positive and negative around the steady-state (60 Hz for frequency signals), the algorithm counts these crossings. The number of crossings detected is labeled as ($cross$) and compared with the crossings detected (ref_c). . After the first three crossings are detected (this guarantees at least one cycle of the oscillating signal), the fast Fourier transform (FFT) is applied to the frequency signals using a rectangular window whose length is defined by the number of samples between the first and the last crossing detected. Then, the dominant oscillatory frequency (f_d) with the greatest magnitude is captured from the Fourier coefficients, computing its variation (Δf_d) when a new crossing is detected. This process is carried out until the frequency variation at the q-th crossing reaches the convergence criterion $\Delta f_d = 1 \times 10^{-3}$, ensuring the optimal window length and minor changes in oscillatory frequencies. Finally, the length of the identification window is determined using the period between the disturbance instant (t_{dist}) and when the last crossing indicates that the dominant frequency does not change.

Algorithm 1 Disturbance time detection via the Teager-Kaiser energy operator

Require: One selected signal of the buffer $freq(1:m,1:k)$ (m is the number of signals) and a time vector $tact(1:k)$ at the k-th current time. The length ls_w of the sliding window s_w. The energy variation accepted tk_c.

Ensure: $k \geq ls_w$. ▷ Where $ls_w = 3$ for the second order operator.

1: The sliding window s_w is defined as $freq(1,k-ls_w:k)$.
2: Compute the energy of s_w at the current time, such as: ▷
$$\Psi[s_w(k)] = s_w^2(2) - s_w(3)s_w(1) \tag{10}$$
3: **if** $\Psi[s_w(k)] > tk_c$ **then**
4: $t_{dist} = tact(p)$; ▷ p is the last sample
5: **end if**

return t_{dist}, p

Algorithm 2 Detection of signal crossings by the steady state.

Require: The current sample k of m frequency signals stored in the buffer $freq(1:m,k)$ and the current simulation time stored in vector $tact(k)$ after the event detection time t_{dist} that corresponds to p. The convergence criterion of frequency variation is defined as Δf_{dc}. The number of crossings detected in previous stages of simulation ref_c. z stands for an index within $1:m$ associated with a selected signal in the buffer $freq(1:m,1:k-p)$.

Ensure: $k-p \geq 2$ ▷ At least 2 samples stored into $ident_w$

1: $ref = 0$; $cross = 0$; $T_{id} = 0$; ▷ Initialization
2: $q = k-p$;$\forall k > p$;$ident_w(1:m,q) = freq(1:m,k)$; $ident_t(q) = tact(k)$;
3: $st = ident_w(z,1:q) - movmean(ident_w(z,1:q))$;
4: **for** i=1,i++,q-1, **do**
5: **if** $ref > st(i) \,\&\, ref < st(i+1)$ **then** ▷ Crossing down
6: $cross = cross+1$;
7: **end if**
8: **if** $ref < st(i) \,\&\, ref > st(i+1)$ **then** ▷ Crossing up
9: $cross = cross+1$;
10: **end if**
11: **if** $cross > 3 \,\&\, cross > ref_c$ **then** ▷ New crossing detected
12: $ref_c = cross$;
13: $f_d(cross) = max(abs(\text{fft}(ident_w(1:m,1:i+1))))$;
14: $\Delta f_d(cross) = f_d(cross) - f_d(cross-1)$;
15: **if** $\Delta f_d(cross) < \Delta f_{dc}$ **then** ▷ Convergence reached
16: $t_{end} = ident_t(q)$;
17: **end if**
18: **end if**
19: **end for**

return ref_c, t_{end}

D. Generalized realization via system identification

The one responsible for precisely identifying the black-box model of the power grid is the eigensystem realization algorithm (ERA). This is a multiple-input multiple-output modal identification algorithm that involves the system realization theory for the construction of state-spaces models ($[\hat{\mathbf{A}}, \hat{\mathbf{B}}, \hat{\mathbf{C}}, \hat{\mathbf{D}}]$) of linear systems. The ERA is based on the singular value decomposition (SVD) of the Hankel matrix $\mathbf{H}_0$ associated with the ringdown behavior of a linear system [5]. A pseudo-code for the Multi-Channel ERA method is detailed in **Algorithm 3**.

III. On-line system identification architecture

This investigation adopts a compound architecture considering two environments: DIgSILENT PowerFactory™ and Matlab™. The former is in charge of performing electromagnetic transient simulations (EMT) at a sampling rate of 10kHz; here, the DIgSILENT programming language (DPL) is used to simulate transmission systems when they are subjected to faulty conditions (inception time and duration are considered), and to communicate with the Matlab™ environment. The DPL is also responsible to produce disjoint data packages each 20ms containing instantaneous secondary voltage values for all generation buses to be sent to Matlab™. In turn, the latter embeds five routines to receive and process the data, which are: synchrophasor data and frequency computation, disturbance time detection, dominant mode's optimal frequency, identification, and frequency response (FR). These routines are described in the following and depicted by the flowchart in Fig. 1.

A. Instantaneous data

Instantaneous secondary voltages of all-generation buses are simultaneously collected by a measuring stage equipped with a capacitive voltage transformer (CVT) installed per phase at each bus. So, instantaneous data consisting of secondary measurements is

Algorithm 3 Multi-Channel Eigensystem Realization Algorithm.

Require: A set of m time-series data of recorded signal $y(k)$ inside the buffer $ident_w$ from t_{dist} to t_{end}, with N samples each one.

Ensure: $p=\frac{N}{2}-1$. ▷ Where p is the size of the Hankel submatrix $\mathbf{H}^{\{q\}}$, this choice assumes that the number of data points is sufficient such that $r>n$.

1: To construct the $\mathbf{Y}_m$ matrix with all recorded signals $y(k)$ ▷

$$\mathbf{Y}_m=\begin{bmatrix} y^{\{1\}} & y^{\{2\}} & \cdots & y^{\{q\}} & \cdots & y^{\{m\}} \end{bmatrix} \tag{11}$$

2: To construct the Hankel matrix $\tilde{\mathbf{H}}_0$ by the rows of $\mathbf{Y}_m$ ▷

$$\tilde{\mathbf{H}}_0=\begin{bmatrix} Y_1^T & Y_2^T & \cdots & Y_p^T \\ Y_2^T & Y_3^T & \cdots & Y_{p-1}^T \\ \vdots & \vdots & \ddots & \vdots \\ Y_p^T & Y_{p-1}^T & \cdots & Y_{p+\gamma}^T \end{bmatrix} \tag{12}$$

where p and γ are integers such that $\gamma>p$.

3: To construct the shifted Hankel matrix $\tilde{\mathbf{H}}_1$

4: To apply SVD method ▷

$$\tilde{\mathbf{H}}_0=\tilde{\mathbf{U}}\tilde{\mathbf{\Sigma}}\tilde{\mathbf{V}}^T \tag{13}$$

5: To separate $\tilde{\mathbf{H}}_0$ into two components, a n large (nonzero in the case of noiseless measurements) and s small (zero in the case of noiseless measurements) singular values ▷

$$\tilde{\mathbf{H}}_0=\begin{bmatrix}\tilde{\mathbf{U}}_n & \tilde{\mathbf{U}}_s\end{bmatrix}\begin{bmatrix}\tilde{\mathbf{\Sigma}}_n & 0\\ 0 & \tilde{\mathbf{\Sigma}}_s\end{bmatrix}\begin{bmatrix}\tilde{\mathbf{V}}_n^T\\ \tilde{\mathbf{V}}_s^T\end{bmatrix} \tag{14}$$

6: To approximate the high-rank Hankel matrix $\tilde{\mathbf{H}}_0$ by a reduced-rank n matrix ▷

$$\tilde{\mathbf{H}}_0\approx\tilde{\mathbf{U}}_n\tilde{\mathbf{\Sigma}}_n\tilde{\mathbf{V}}_n^T \tag{15}$$

7: To compute the discrete system matrices $\hat{\mathbf{A}}$, $\hat{\mathbf{B}}$, $\hat{\mathbf{C}}$, and $\hat{\mathbf{D}}$ ▷

$$\begin{aligned}\hat{\mathbf{A}}&=\tilde{\mathbf{\Sigma}}_n^{-\frac{1}{2}}\tilde{\mathbf{U}}_n\tilde{\mathbf{H}}_1\tilde{\mathbf{V}}_n^T\tilde{\mathbf{\Sigma}}_n^{-\frac{1}{2}} & \hat{\mathbf{B}}&=\tilde{\mathbf{\Sigma}}_n^{\frac{1}{2}}\tilde{\mathbf{V}}_n(1:n,1:n)\\ \hat{\mathbf{C}}&=\tilde{\mathbf{U}}_n(1:N,1:n)\tilde{\mathbf{\Sigma}}_n^{\frac{1}{2}} & \hat{\mathbf{D}}&=y_0\end{aligned} \tag{16}$$

return $\hat{\mathbf{A}}$, $\hat{\mathbf{B}}$, $\hat{\mathbf{C}}$ and $\hat{\mathbf{D}}$

assembled in a matrix array containing 200 samples (a period of 20 ms) and all three-phase secondary voltages of all generation buses.

B. Synchrophasor data and frequency computation

Prior to processing all instantaneous data, the positive sequence of each bus is extracted from the three-phase secondary signals via Fortescue's theorem; then all positive sequence signals are converted into small pieces of phasor quantities. This is achieved via the multi-channel processing feature of the DFT in the analysis equation (1). Then, frequency computations in (3) are performed according to the synchrophasor norm. Finally, each frequency data is stored in a virtual PDC created by a buffer termed $freq$, where the i-th instantaneous package is associated with the i-th synchrophasor package.

C. Disturbance time detection

This routine examines each frequency data using the **Algorithm 1**. For this purpose, a 3-sample buffer is created aiming to find the right disturbance instant (t_{dist}) subjected to the threshold fixed (tk_c). According to our investigation, this threshold is signal-dependent, therefore is associated with the input signals used for identification purposes, so other users may use historical data to determine it previously.

D. Identification routine

This routine executes the **Algorithm 3** over the range defined by the identification window, starting from t_{dist} and ending when T_{id} is elapsed. Thus, Markov's parametric matrices ($\hat{\mathbf{A}}$, $\hat{\mathbf{B}}$, $\hat{\mathbf{C}}$, $\hat{\mathbf{D}}$) forming a state-space model representation are achieved, ensuring that the dominant mode's optimal frequency is successfully captured. For comparison purposes, the multiple-channel matrix pencil is also implemented according to [5].

E. System frequency response

The frequency response is computed using the identified state-space form computed by the **Algorithm 3** and is compared against the multiple-channel matrix pencil. It computes the frequency behavior between a single input and a single output from the state-space model identified. For this purpose, a frequency range is defined within a bandwidth by a starting frequency, a frequency step and an ending frequency, deriving a frequency vector of the form $w_k=2\pi f_{bw}(k)$. Afterward, the magnitude of the output/input system response is derived from the transfer function $\mathbf{H}(j\omega_k)=\hat{\mathbf{C}}(j\omega_k\mathbf{I}-\hat{\mathbf{A}})^{-1}\hat{\mathbf{B}}+\hat{\mathbf{D}}$.

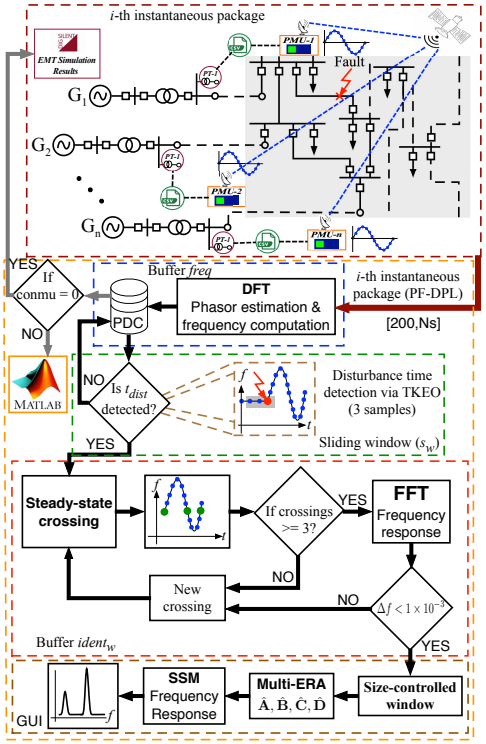

Fig. 1. Real-time simulation architecture.

F. Graphical user interface

The developed platform has a GUI that continuously monitors the frequencies calculated at the generation buses. It allows the visualization of the analysis window's behavior from its creation until it reaches its optimal size. Also, the GUI displays the highest energy singular values found by the **Algorithm 3**, and the frequency response once the power system linear model is identified.

IV. On-line System Identification in Power Systems

As described in the overall architecture in Section III, the first two routines (instantaneous and synchrophasor data) emulate virtual PMUs to provide real-time information to the phasor data concentrator (PDC) that is embedded in the Matlab™ environment. The next three routines are fed by the synchrophasor information available in the PDC. Thus, an online system identification can be achieved on any power system subjected to the computational resources of the host running the application.

A. Test system

The 39-bus NEPS shown in Fig. 2 is selected as test system. It contains 10 generators, 19 loads, 34 transmission lines, and 12 transformers. The NEPS represents a simplified model of the transmission system located in the Northeastern USA. Its nominal frequency is 60 Hz and the main grid voltage is 345kV (rated voltage) [19].

To obtain the signals from the simulation, a 3-cycle three-phase short circuit is applied to the transmission line connected between

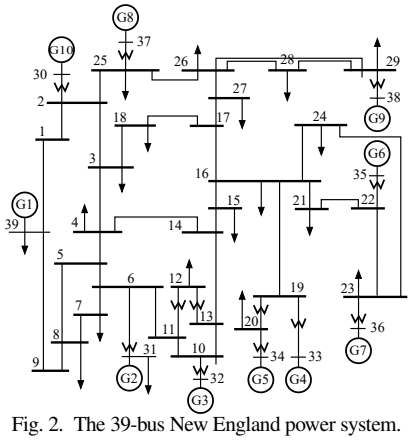

Fig. 2. The 39-bus New England power system.

Card Street (bus 14) and Sherman Road (bus 15) substations at $t=0.5$s. The fault clearing time is defined as $t_c=0.05$s. When the system is subjected to this disturbance for 0.05s, the stability is preserved [19], [20], [21]. This is intended to stimulate the oscillatory modes and to identify the power system linear model.

B. Online Identification on the NEPS

To run our platform, a total simulation time of 20s is defined and the NEPS runs over DIgSILENT PowerFactory™ . The instantaneous phase-to-ground voltages are measured by the CVTs installed at the generation buses 30 to 39 and are sampled using $\Delta t_1=0.1ms$, thus the results of the EMT simulation have a sampling frequency $Fs_1=1/\Delta t_1=10kHz$. Every package containing 200 samples is stored in csv format together with the time vector associated with the data.

Matlab™ loads and transforms the set of instantaneous voltage data per phase into their respective phasors, using (1), (2), (3) and (4). This process guarantees that the voltage phasors are obtained with time intervals of $\Delta t_2=20ms$, or a sampling frequency of 50 Hz.

The nodal voltage phasors contain the necessary information to carry out the identification process. These values allow the computation of the frequency measured at the system nodes and the simulation of PMUs installed at these points.

Once the voltage phasors have been estimated and the frequencies computed at each node as appropriate, the type of selected signal begins to be stored in the $freq$ buffer. This buffer grows with each new frequency computation. The length of this buffer determines the current iteration of the simulation $iter$.

For this study case, the computed frequency at bus 39 is selected to apply the **Algorithm 1**. For detecting a three-phase short-circuit in the NEPS, the tk_c value is set to 15 Hz^2, where Hz^2 is the result of calculating $[Hz^2]$ from the frequency signal using (9). The energy change of the computed frequency signal at bus 39 during that fault is shown in Fig. 3.

In this scenario, the setting value is overcome at $t=$0.5199 s. As can be seen, the energy changes in the signal continue while the fault remains in the system. The energy change again decreases to near zero after a short time interval. These significant changes in the energy variation correspond to the transient state after the fault is applied and until is released. After 100ms of the energy change is detected, that is, 5 samples each every 20ms, the $ident_w$ buffer is created, and the transient state is removed for subsequent analyses.

Since the identification buffer is created, it grows with each new frequency computation after the transient effect. The $freq$ buffer continues working in parallel. With the data stored in $ident_w$ buffer, **Algorithm 2** is executed to determine the end time of the identification window.

With each new crossing by the steady-state of the computed frequency at bus 30, the FFT is applied to all the signals in the $ident_w$ buffer. This bus is randomly selected to show the facilities offered by the developed platform. Then, the variation of the dominant frequency is analyzed after at least three crossings are detected. Figure 4 exhibits the behavior of the dominant frequency variation during the simulation.

The threshold for the convergence criterion of the dominant frequency variation for finding the optimal number of crossing is set to 1×10^{-3}Hz. As can be seen in Fig. 4, this value is reached at the 13-th crossing by the steady-state of the selected signal. In this way, the ending time instant of the identification window in the simulation

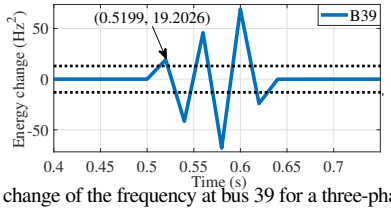

Fig. 3. Energy change of the frequency at bus 39 for a three-phase short circuit.

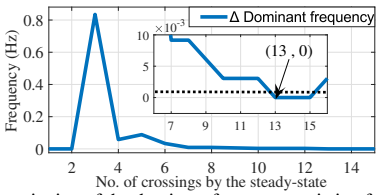

Fig. 4. Convergence criterion of the dominant frequency variation for finding the optimal number of crossing to select the right analysis window.

is indicated in Fig. 5. Thus, the identification window comprises from $t_{ini}=0.6199s$ up to $t_{end}=10.9799$ s, resulting in a window size of $t_{window}=10.36$ s that is equivalent to 519 samples.

After determining the length of the identification window, the **Algorithm 3** performs the extraction of the power system linear model. The identification process is carried out using an energy criterion set to 99% in the same way as in [5]. The first singular values calculated under this setting and their energy are observed in Fig. 6. Only the first 11 singular values are used for the identification of the NEPS linear model as shown in Fig. 6(a). The energy associated with them represents 98.479% of the total values found, as observed in Fig. 6(b) . The following singular values are not representative in terms of their low energy, reducing the model order.

The resulting power system linear model in discrete-time and in accordance with (16) and the multiple Matrix Pencil method has the following dimensions $\hat{\mathbf{A}}\in\mathbb{R}^{11\times11}$, $\hat{\mathbf{B}}\in\mathbb{R}^{11\times10}$, $\hat{\mathbf{C}}\in\mathbb{R}^{10\times11}$, and $\hat{\mathbf{D}}\in\mathbb{R}^{10\times10}$. Thus, the system is modeled using 11 states, 10 inputs, and 10 outputs. All matrices are transformed into continuous time form by using a zero-order hold method to assemble the state-space representation and execute the system frequency response routine.

The frequency responses in Figs. 7(a) and 8 are computed employing the frequency vector $f_k=[0.1:0.001:1.5]$. For the sake of brevity, these just represent the output/input transfer functions associated with the frequency of generators G1-G4 as output to a unit impulse as input, respectively. It is remarkable that the dominant frequency of 0.62 Hz is correctly captured by all transfer functions in all responses, which is also corroborated in Fig. 7(b) where continuous spectra are taken for the transfer function of G1 using from 3 crossings up to 13. Notice that during the first crossings exist notable differences in the frequency response and near the 13-th crossing where the dominant frequency does not change anymore. Then, the frequency response from the state-space model converges at the same time as the dominant frequency variation obtained by applying the FFT to the $ident_w$ buffer.

For comparison purposes, we also implement the identification routine with the well-known matrix pencil method in a multiple-

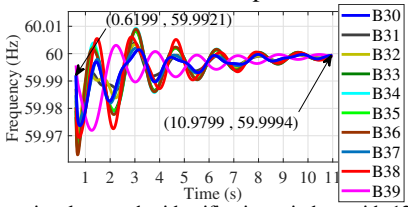

Fig. 5. Frequency signals over the identification window with 13 crossings by the steady-state in the frequency signal at bus 30.

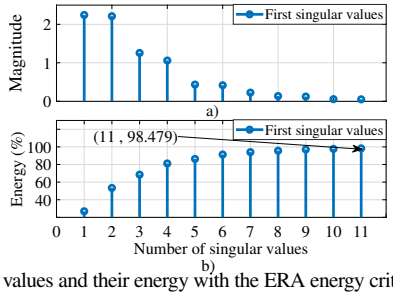

Fig. 6. Singular values and their energy with the ERA energy criterion set to 99%.

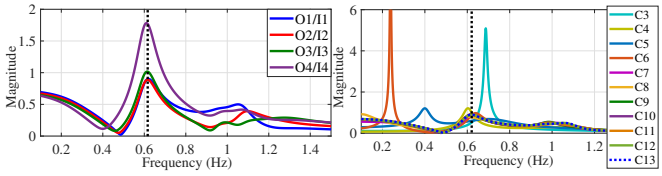

(a) (b)

Fig. 7. Frequency responses of the: (a) output/input transfer functions associated with the frequency of generators G1-G4 as outputs (O1-O4); and (b) transfer function O1/I1 associated with G1 until the 13-th crossing.

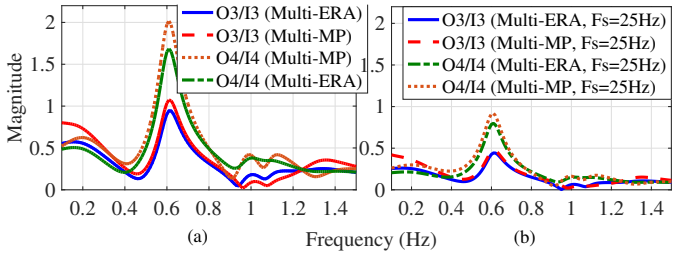

(a) (b)

Fig. 8. Comparisons of frequency responses between Multiple-ERA and Multiple-Matrix Pencil for 2-outputs and 2-inputs in the New England power grid. (a) Output 3/ Input 3 using a sampling frequency of 50Hz; (b) Output 4/ Input 4 using a sampling frequency of 25Hz.

channel processing way to identify the power system linear model. After performing its evaluation on our platform by varying the sampling rate, the frequency response for the linear models derived is plotted in Fig. 8. Where Fig. 8(a) exhibits the transfer function between Output 3 and Input 3 of generator G3 using a sampling frequency of 50Hz; whereas Fig. 8(b) displays the transfer function between Output 4 and Input 4 of generator G4 using a sampling frequency of 25Hz. As expected, both identification routines preserve similar energy as the same sampling rate is used. When different sampling rates are used from different sensors/PMUs, the PDC can deal with this issue.

This online platform is also supported by a GUI developed in Matlab™ . It displays the real-time results attained at each stage. Each data package is plotted in the real-time measurement graph during each simulation instant. In the same way, the analysis window graph plots the frequency measurements at all generation buses after the disturbance is detected and it stops when the optimal size is reached. The graphs corresponding to the system frequency response and the most significant singular values are shown after the power system linear model is found. All computations are achieved using DIgSILENT PowerFactory™ and Matlab™ based environments in a desktop running Windows 10 with Intel(R) Xeon(R) CPU E5-1620 v4, 3.5 GHz, 32 GB RAM, and 64-bit. The code for the algorithms is online available in [22].

V. Conclusions

This investigation has developed and implemented a testing architecture for online system identification approaches. This research platform profits from the use of two well-known computational programs to demonstrate its performance and effectiveness for optimally identifying a large-scale power system. To ensure a reliable and optimal system identification, this platform takes advantage of a mutually beneficial relationship among four well-established mathematical techniques, this symbioses guarantees the estimation of synchrophasor information, the correct detection of the right disturbance instant, the optimal extraction of the dominant frequency, and the proper identification of the Markov parameters that assemble the descriptor form of Multiple-Input and Multiple-Output (MIMO) linear systems for modeling modern power grids. Likewise, this platform integrates the computation of a centered moving average by sliding a window and the automatic detection of the steady-state crossings to effectively determine the optimal and adaptable identification window.

The implemented window size optimal selection method ensures that the dominant frequency is detected before the identification process is conducted.

Numerical results unveil the potential for recreating the real behavior of power systems; in particular, the proposed architecture can deal with any system identification technique to be tested.

Future works would contemplate the inclusion of online control structures with parameters' online tuning.

References

[1] N. Hatziargyriou and et al, "Definition and classification of power system stability – revisited extended," *IEEE Trans. Power Systems*, vol. 36, no. 4, pp. 3271–3281, 2021.

[2] P. Tielens and D. Van Hertem, "The relevance of inertia in power systems," *Renew. Sust. Energ. Rev.*, vol. 55, pp. 999–1009, 2016.

[3] X. Zhang and et al, "A review on wide-area damping control to restrain inter-area low frequency oscillation for large-scale power systems with increasing renewable generation," *Renew. Sust. Energ. Rev.*, vol. 57, pp. 45–58, 2016.

[4] J. A. de la O Serna, "Dynamic phasor estimates for power system oscillations," *IEEE Trans. Instrum. and Meas.*, vol. 56, no. 5, pp. 1648–1657, 2007.

[5] J. Sanchez-Gasca and et al, "Identification of electromechanical modes in power systems," in *IEEE Task Force Report, Special Publication TP462*. IEEE, 2012.

[6] M. Hatami and et al, "Online transfer function estimation and control design using ambient synchrophasor measurements," *IEEE Trans. Power Systems*, 2022.

[7] H. Liu and et al, "Armax-based transfer function model identification using wide-area measurement for adaptive and coordinated damping control," *IEEE Trans. Smart Grid*, vol. 8, no. 3, pp. 1105–1115, 2015.

[8] J. Zhang and et al, "A novel adaptive wide area pss based on output-only modal analysis," *IEEE Trans. Power Systems*, vol. 30, no. 5, pp. 2633–2642, 2015.

[9] J. Kaiser, "On a simple algorithm to calculate the 'energy' of a signal," in *I. Conf. on Acous., Speech, and Signal Proces.*, 1990, pp. 381–384 vol.1.

[10] A. Zamora-Mendez and et al, "Electromechanical modes identification based on an iterative eigenvalue decomposition of the hankel matrix," *IEEE Trans. Power Systems*, pp. 1–1, 2022.

[11] J. Dobrowolski, F. Segundo, M. Paternina *et al.*, "Inter-area oscillation control based on eigensystem realization approach," in *2018 IEEE International Autumn Meeting on Power, Electronics and Computing (ROPEC)*. IEEE, 2018, pp. 1–6.

[12] L. Fu and et al, "A multiple frequency taylor model-based dynamic synchrophasor estimation algorithm," *IEEE Trans. Smart Grid*, vol. 10, no. 6, pp. 6870–6882, 2019.

[13] C. Toledo-Santos and et al, "Building up a wide-area protection system simulator," in *2020 52nd NAPS*. IEEE, 2021, pp. 1–6.

[14] "Ieee standard for synchrophasor measurements for power systems," *IEEE Std C37.118.1-2011 (Revision of IEEE Std C37.118-2005)*, pp. 1–61, Dec 2011.

[15] IEEE, "IEEE Standard for Synchrophasor Measurements for Power Systems – Amendment 1: Modification of Selected Performance Requirements," *IEEE Std C37.118.1a-2014 (Amendment to IEEE Std C37.118.1-2011)*, pp. 1–25, April 2014.

[16] I. Kamwa, A. K. Pradhan, and G. Joós, "Robust detection and analysis of power system oscillations using the teager-kaiser energy operator," *IEEE Trans. Power Syst.*, vol. 26, no. 1, pp. 323–333, 2010.

[17] H. M. Teager and S. M. Teager, "Evidence for nonlinear sound production mechanisms in the vocal tract," in *Speech Production and Modelling*, vol. 55. Springer Netherlands, Jul 1989, pp. 17–29.

[18] P. Maragos and A. Potamianos, "Higher order differential energy operators," *IEEE Sig. Proc. Letters*, vol. 2, no. 8, pp. 152–154, 1995.

[19] M. A. Pai, *Energy function analysis for power system stability*. Springer Science & Business Media, 2012.

[20] M. Eremia and M. Shahidehpour, *Handbook of electrical power system dynamics: modeling, stability, and control*. John Wiley & Sons, 2013, vol. 92.

[21] D. PowerFactory, "Bus new england system," *Heinrich-Hertz-Str*, vol. 9, p. 72810, 39.

[22] J. Moreno and et al, "On-line system identification of power system linear models," 2022, (accessed October 12, 2022), https://github.com/jamcorbea/On-Line-System-Identification-of-Power-System-Linear-Models.git.